ISSN 1063-7850, Technical Physics Letters, 2020, Vol. 46, No. 8, pp. 787–791. © Pleiades Publishing, Ltd., 2020.
Russian Text © The Author(s), 2020, published in Pis'ma v Zhurnal Tekhnicheskoi Fiziki, 2020, Vol. 46, No. 16, pp. 7–11.

An Ultra-Wideband Stripline Bandpass Filter with a Noise Suppression Level of More than 100 dB

B. A. Belyaev[a,b]*, A. M. Serzhantov[b], An. A. Leksikov[a], Ya. F. Bal'va[a], and E. O. Grushevskii[a]

[a] *Kirensky Institute of Physics, Krasnoyarsk Scientific Center, Siberian Branch, Russian Academy of Sciences, Krasnoyarsk, 660036 Russia*

[b] *Siberian Federal University, Institute of Engineering Physics and Radio Electronics, Krasnoyarsk, 660041 Russia*

**e-mail: belyaev@iph.krasn.ru*

Received April 27, 2019; revised April 27, 2020; accepted May 6, 2020

Abstract—An ultra-wideband bandpass filter formed by cascading of a novel high-pass filter (HPF) and a low-pass filter (LPF) on suspended substrates with a two-sided pattern of strip conductor has been investigated. The high selectivity of the HPF is ensured by the transmission zeros near the passband, the number of which is equal to the filter order. A second-order HPF has been designed on a 0.5-mm-thick substrate with a permittivity of $\varepsilon = 9.8$ using the numerical electrodynamic analysis of a 3D model of the filter. The experimental HPF prototype has a cutoff frequency of $f_b = 0.25$ GHz at a level of -3 dB and a passband that extends to 5 GHz. The ultra-wideband bandpass filter formed by cascading of the LPF and the designed HPF has a fractional bandwidth of $\Delta f/f_0 = 150\%$ with a central frequency of $f_0 = 1$ GHz. It has the broad and deep high-frequency stopband, which extends to a frequency of $7.8f_0$ at a suppression level of -100 dB.

Keywords: passband filter, resonator, dielectric substrate, strip conductors.

DOI: 10.1134/S1063785020080179

Frequency-selective microwave devices, including bandpass filters (BPFs), are among the most important components of communication, radar, and radio navigation systems and various types of measuring and specialized radio equipment [1, 2]. In recent years, much attention of radio engineers has been paid to ultra-wideband (UWB) filters. The use of ultra-wideband signals increases the data transmission rate, which, as is known, is directly related to the working frequency bandwidth.

A well-known approach to designing UWB filters is based on the enhancement of couplings between resonators via partial removal of metallization in the grounded base [3]. In addition, UWB filters based on short-circuit stubs [4] and multimode resonators [5] are widely used. The common drawbacks of these approaches are, first, the complexity of implementing filters with relative bandwidths of more than 120% and, second, a relatively narrow high-frequency stopband of these devices, which extends, at best, to a frequency of $\sim 4f_0$ at an attenuation level of merely ~40 dB. It should be noted that the overwhelming majority of the available UWB filter designs cannot be screened because of the occurrence of spurious volume resonances to the housing near the passband. The unscreened filters can interfere with other components of the radio modules, which causes electromagnetic incompatibility. The above-mentioned difficulties can be overcome, to a certain extent, by cascading of a high-pass filter (HPF) and a low-pass filter (LPF) in the UWB filter design [6, 7]. Obviously, to obtain a high BPF performance, it is necessary to ensure a high selectivity of LPFs and HPFs. In particular, the LPF should have not only steep slopes of its frequency response, but also a broad and deep stopband, as, for example, in the filter proposed in [8]. At the same time, the HPF should have a broad passband at the steep low-frequency slope of the frequency response.

This Letter reports on the creation of a high-selectivity UWB BPF on the basis of a novel HPF designed on a dielectric substrate suspended in a metal casing with a two-sided pattern of strip conductors. To understand the operation principle of this HPF, we consider the simplest filter design (Fig. 1). It consists of two identical rectangular strip conductors on the upper side of a substrate with length l_2 and width W with the connected input and output filter ports. On the substrate downside, exactly beneath it, there is a rectangular strip conductor the center of which is connected to a narrow strip conductor with length l_1 and width w, which is closed to the screen on its opposite end (Fig. 1). The proposed design differs from the known solutions by an additional coupling between its input and output, which is ensured by narrow capaci-

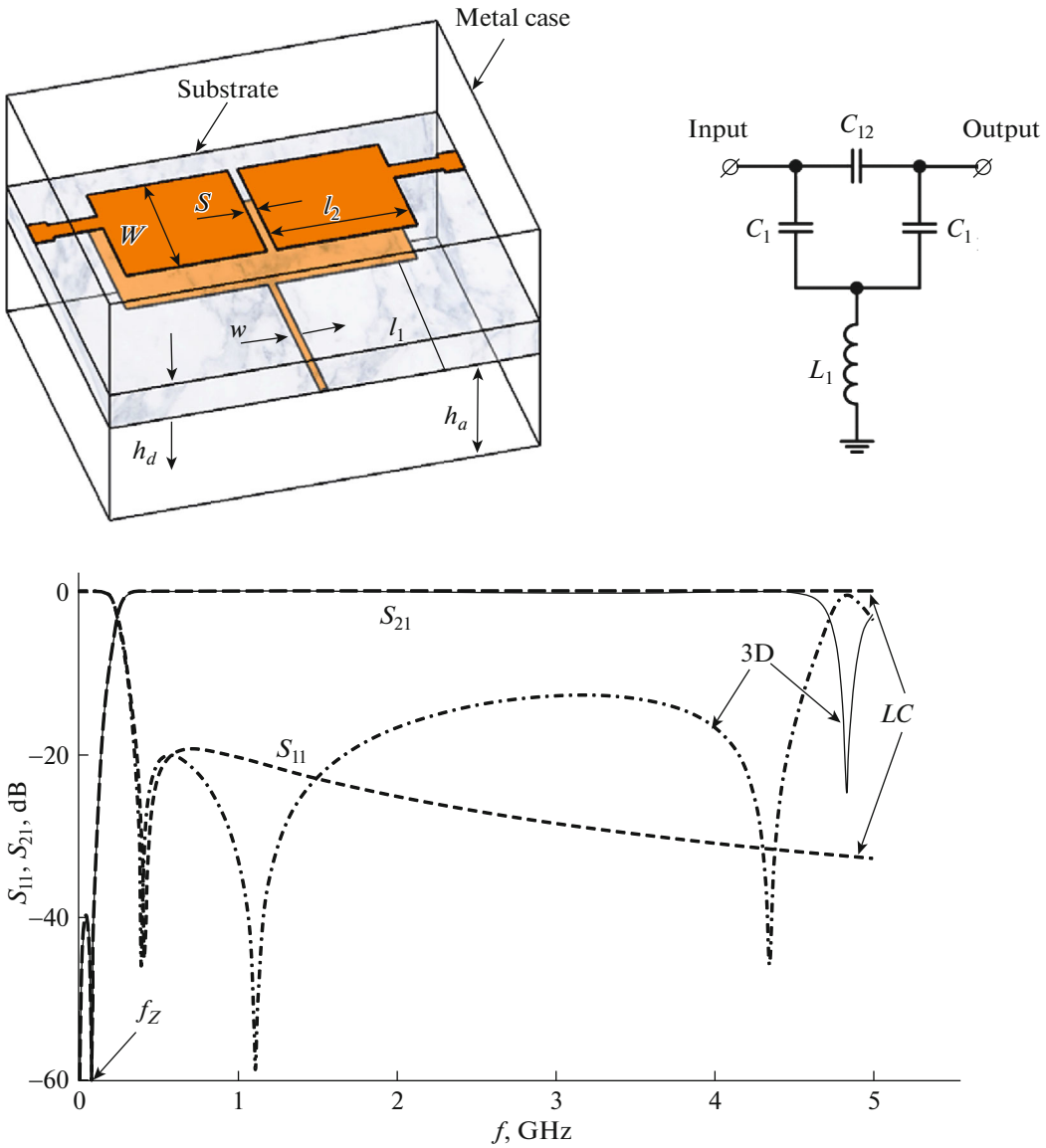

Fig. 1. Design of the stripline high-pass filter and its frequency response (solid and dash-and-dot lines) and equivalent circuit of the first-order high-pass filter and its frequency response (dashed lines).

tive gap S between the conductors on the upper side of the substrate.

Figure 1 (solid line) shows the filter frequency response calculated using the numerical electrodynamic analysis of a 3D model of the filter. The design parameters used in the model are a substrate thickness of $h_d = 0.5$ mm, a substrate permittivity of $\varepsilon = 9.8$, a distance of $h_a = 5$ mm between the upper and lower screens and the corresponding substrate surfaces, strip conductor widths of $w = 0.12$ mm and $W = 6.5$ mm and lengths of $l_1 = 19$ mm and $l_2 = 7.22$ mm, and a gap of $S = 0.25$ mm between the wide conductors. The frequency response contains an attenuation pole (transmission zero) near the passband at a frequency of f_Z, which significantly increases the slope of the HPF response. It is convenient to analyze the origin of this feature in the frequency response using the equivalent circuit of the investigated filter with lumped elements (see Fig. 1). The circuit consists of an inductance and three capacitors. The validity of the equivalent circuit is proved by the almost complete coincidence of the frequency dependence of its transmission loss S_{21} (dashed lines) with the characteristic obtained by the electrodynamic calculation of the filter 3D model. Note that the values of elements of the HPF equivalent circuit ($L_1 = 20.88$ nH, $C_1 = 9.41$ pF, and $C_{12} = 0.5$ pF) were obtained by analyzing a one-dimensional model of the filter in the quasi-static approximation.

The presented HPF design corresponds to a first-order filter, which is confirmed by the presence of the only minimum in the frequency dependence of reflection loss S_{11} in the equivalent circuit passband. This minimum coincides with the first minimum in the frequency dependence of S_{11} in the passband of the filter 3D model. The two additional minima in the $S_{11}(f)$ dependence of the 3D model are obviously caused by resonances of the higher oscillation modes of the strip structure. The analysis of the equivalent circuit shows that transmission zero frequency f_Z in the stopband is independent of the wave impedance of the input and output ports and determined by the expression

$$2\pi f_Z = \omega_0 K_C, \quad (1)$$

where $\omega_0 = 1/\sqrt{2L_1C_1}$ is the eigenfrequency of the oscillatory circuit at the grounded input and output of the equivalent circuit and $K_C = \sqrt{2C_{12}/(C_1 + 2C_{12})}$ is the coefficient of the capacitive coupling between the input and the output. It follows from formula (1) that frequency f_Z is proportional to K_C, i.e., can change in a wide range upon variation in capacitance C_{12}, depending on gap size S. This fact allows the filter to deeply suppress noise at a specified frequency. It is worth noting that the origin of the attenuation pole at frequency f_Z is related to the mutual compensation of antiphase modes of the same amplitude passing from the input to the output of the device through two "channels" [9]. In this design, one of the channels of signal transmission between the ports is obviously formed by capacitance C_{12} and the other, by the chain C_1, L_1, and C_1.

Figure 2 shows the design of the proposed second-order HPF and its equivalent circuit. This filter has a higher selectivity. In the frequency response of its 3D model calculated in the electrodynamic analysis program (solid line), there are already two transmission zeros at frequencies f_{Z1} and f_{Z2}, which are caused by the inductive coupling between narrow strip conductors. Indeed, analysis of the equivalent circuit (Fig. 2) yielded the expression for the transmission zero frequencies:

$$2\pi f_{Z1,2} = \frac{\omega_0 K_C}{\sqrt{1-K_L^2}} \times \sqrt{1 + K_L\frac{C_1}{C_{12}} \mp \sqrt{K_L^2\left(1+\frac{C_1^2}{C_{12}^2}\right) + 2K_L\frac{C_1}{C_{12}}}}, \quad (2)$$

where $K_L = L_{12}/L_1$ is the inductive coupling coefficient of the circuits. It can be seen that, in the absence of the inductive interaction ($K_L = 0$), the frequencies of zeros degenerate and the frequency response of the circuit contains one transmission zero, the frequency of which coincides with Eq. (1). At $K_L > 0$, the transmission zero frequencies split; the splitting increases with the K_L value. The investigations showed that the number of gain zeros in the higher-order HPF designs corresponds to the filter order. Figure 2 shows the frequency dependence of the reflection coefficient of the filter (dash-and-dot line) and the same characteristic for the equivalent HPF circuit calculated at element ratings of $L_1 = 20$ nH, $C_1 = 12.2$ pF, $C_{12} = 0.28$ pF, and $L_{12} = 0.044$ nH (dashed line). The frequency response for the equivalent circuit is not shown, since, on the figure scale, it does not differ from the dependence obtained using the electrodynamic analysis of the 3D model (solid line) up to the upper limit of the passband.

Note that the parametric synthesis of the investigated stripline HPF (Fig. 2) was performed using the numerical electrodynamic analysis of its 3D model in the CST Studio Suite program by selecting the sizes of the topology of strip conductors of the structure on alumina ceramic substrate with a permittivity of $\varepsilon = 9.8$ and a thickness of $h_d = 0.5$ mm. The parameters of the synthesized filter are strip conductor widths of $w = 0.12$ mm and $W = 10.8$ mm and lengths of $l_1 = 17.5$ mm, $l_2 = 8.42$ mm, and $l_3 = 15.3$ mm; gaps of $S = 0.4$ mm; a distance of $l_{12} = 19.53$ mm between narrow conductors; and a distance of $h_a = 5$ mm from the upper and lower screens to the substrate surfaces.

The synthesized HPF was fabricated by photolithography to experimentally test the operability of the design. A photograph of the filter is shown in Fig. 2. The filter dimensions are about $38 \times 28 \times 11$ mm^3. The measured frequency dependence of transmission loss $S_{21}(f)$ of the experimental HPF is shown by the dashed line. The filter has a passband cutoff frequency of $f_b = 0.25$ GHz at a level of -3 dB and the high-frequency passband edge of at a level of -3 dB extends to a frequency of $20f_b$. It can be seen that the calculated frequency dependence of transmission loss $S_{21}(f)$ of the HPF is in good agreement with the measured one.

Using a cascade connection of the developed HPF design and the LPF design proposed in [8], we fabricated a UWB BPF with a passband central frequency of $f_0 = 1$ GHz and a passband fractional bandwidth of $\Delta f/f_0 = 150\%$ (see the characteristics in Fig. 3). The solid line in Fig. 3 shows the calculated frequency dependence of filter transmission loss $S_{21}(f)$, and the dotted and dashed lines show the $S_{21}(f)$ dependence and the frequency dependence of reflection loss $S_{11}(f)$ measured on an R&S ZVA40 vector network analyzer with a dynamic range of over 150 dB. It can be seen that the developed BPF has an ultrabroad passband, a large slope of the frequency response, and an extended deep stopband, which reaches a frequency of almost $8f_0$ at a suppression level of 100 dB. The minimum insertion loss in the passband of the fabricated filter is only 0.25 dB at a maximum reflection level of -20 dB in the passband.

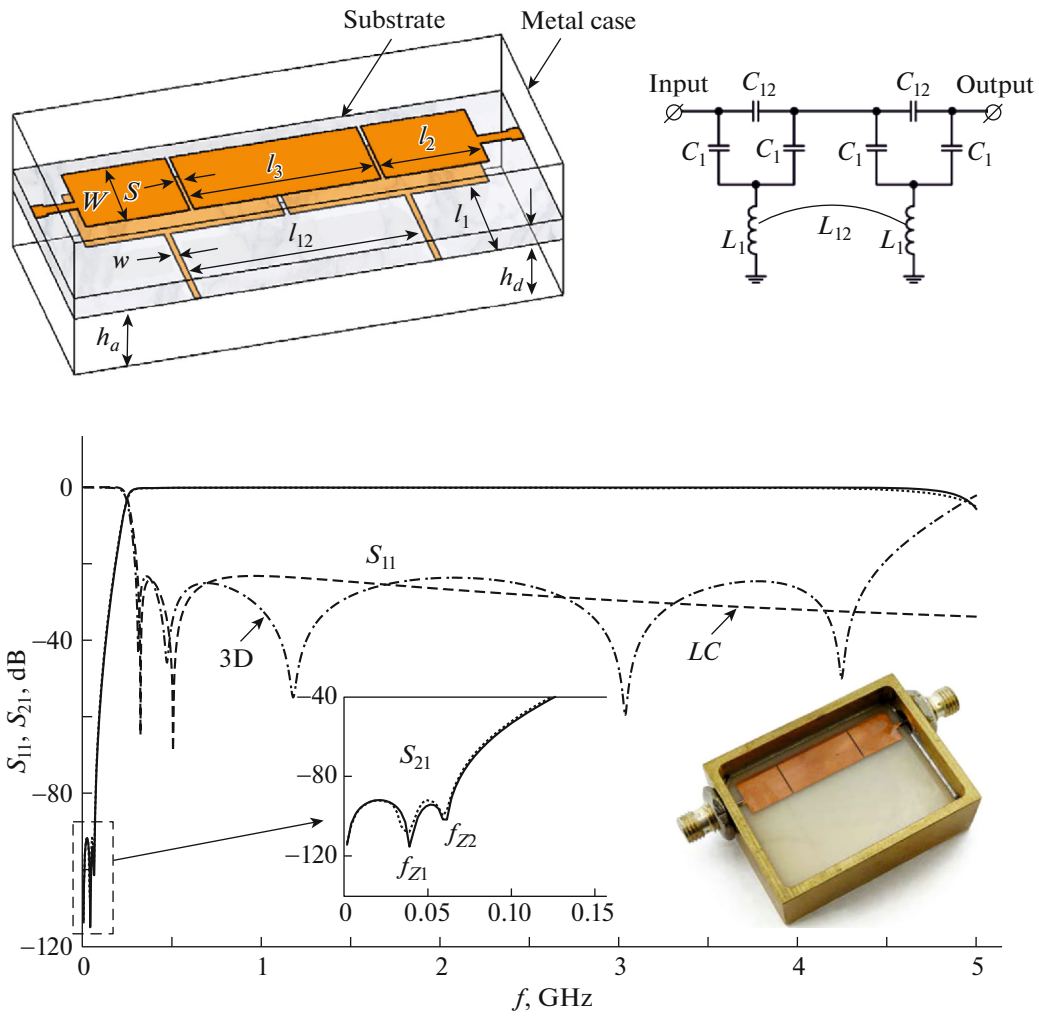

Fig. 2. Design and equivalent circuit of the second-order HPFs and their frequency responses. The solid line corresponds to the $S_{21}(f)$ dependence calculated for the filter 3D model and the dotted line corresponds to the measurement results. For more detailed explanations, see text.

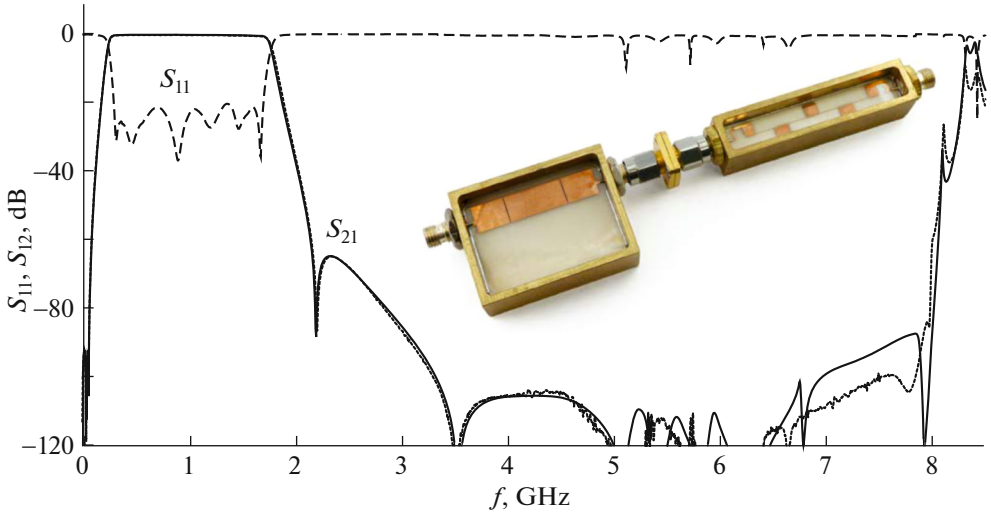

Fig. 3. Frequency response and photograph of the ultra-wideband BPF. The solid line corresponds to the calculation; the dotted and dashed lines correspond to the experiment (see text for more details).

Thus, the investigated new miniature HPF design with a two-sided pattern of strip conductors on a suspended substrate makes it possible to create the high-selectivity BPFs with a fractional bandwidth of up to 150% using simple cascading of the designed filter and a LPF. Such BPFs, due to the presence of transmission zeros near the passband, have steep slopes of the frequency response and a record deep and broad stopband, in comparison with the available stripline designs.

FUNDING

This work was financially supported by the Ministry of Science and Higher Education of the Russian Federation in the implementation of the integrated project "Creation of a production of earth stations of advanced satellite communications systems to ensure the coherence of hard, northern and Arctic territory of Russian Federation," implemented with the participation of the Federal Research Center "Krasnoyarsk Science Center of the Siberian Branch of the Russian Academy of Sciences|" (agreement number 075-11-2019-078 dated 13.12.2019).

CONFLICT OF INTEREST

The authors declare that they have no conflict of interest.

REFERENCES

1. I. C. Hunter, *Theory and Design of Microwave Filters*, Vol. 48 of *IET Electromagnetic Waves Serie*s (Cambridge Univ. Press, Cambridge, 2006).
2. M. A. Morgan, *Reflectionless Filters* (Artech House Microwave Library, Boston, London, 2017).
3. Ya. A. Kolmakov and I. B. Vendik, in *Proceedings of the 35th European Microwave Conference 2005* (2005), Vol. 1, No. 1608783, p. 21.
4. X. Gao, W. Feng, and W. Che, IEEE Microwave Wireless Compon. Lett. **27**, 123 (2017).
5. B. A. Belyaev, A. M. Serzhantov, A. A. Leksikov, Y. F. Bal'va, and An. A. Leksikov, Microwave Opt. Technol. Lett. **62**, 1183 (2020).
6. C.-L. Hsu, F.-C. Hsu, and J.-T. Kuo, in *Proceedings of the IEEE MTT-S International Microwave Symposium* (IEEE, 2005), p. 679.
7. W. Menzel, M. S. R. Tito, and L. Zhu, in *Proceedings of the Asia-Pacific Microwave Conference* (IEEE, 2005), Vol. 4, No. 1606747, p. 1.
8. B. A. Belyaev, A. M. Serzhantov, A. A. Leksikov, Ya. F. Bal'va, E. O. Grushevskii, and S. A. Khodenkov, Tech. Phys. Lett. **46**, 364 (2020).
9. B. A. Belyaev, A. A. Leksikov, A. M. Serzhantov, and V. V. Tyurnev, Prog. Electromagn. Res. Lett. **25**, 57 (2011).

Translated by E. Bondareva